Vibronic Analysis of the ca. 400 nm Band of the Phenoxy Radical within the Approximation of the Weak Coupling Limit

Junko TAKAHASHI* and Tadamasa SHIDA
Department of Chemistry, Faculty of Science, Kyoto University, Kyoto 606-01
(Received January 12, 1994)

The effect of vibronic coupling on the absorption band at ca.400 nm as well as on the Raman spectrum of the phenoxy radical (The IUPAC nomenclature recommends phenoxyl. However, in spectroscopic studies most authors prefer phenoxy to phenoxyl.) is examined by ab initio MO calculations within the framework of the adiabatic approximation. The vibronic coupling effect is represented in terms of the linear non-Condon term in the analysis of the absorption band and in terms of the B-term in the Raman study. The inclusion of the coupling effect improves theoretical spectra fits to experimental spectra.

As discussed in our previous work[1] the phenoxy radical has been studied considerably in the past few decades.[1—13] In particular, a weak and a strong absorption band at about 400 and 300 nm of the radical were studied in comparison with the benzyl radical.[14] In our previous work, the absorption band at about 400 nm of the phenoxy radical was concluded to consist of the two electronic transitions $\tilde{X}\,^2B_1 \rightarrow \tilde{1}\,^2A_2$ and $\tilde{X}\,^2B_1 \rightarrow \tilde{2}\,^2B_1$.[1] The vibronic coupling between the two is considered much weaker than in the benzyl radical, because a simple superposition of the calculated spectra for the two transitions reproduces fairly well the experimental spectrum.[1]

In the present work we have carried out ab initio molecular orbital (MO) calculations including the effect of the vibronic coupling in the weak coupling limit. As a result, the theoretical absorption and Raman spectra are modified favorably in comparison with the experimental Trapped Ion Photodissociation (TIP)[11,12] and resonance Raman[9,10] spectra. In the theoretical Raman spectrum, the contribution of the non-totally symmetric modes is demonstrated.

Method of Calculation

In the adiabatic treatment the vibronic transition dipole moment is evaluated by expanding the integral for the dipole moment by a Taylor series in terms of the normal modes, after completion of the integration over the electronic coordinated as given in Eq. 1.[15—17]

$$\begin{aligned}\left\langle \tilde{G}\{n\} \mid M \mid \tilde{E}\{m\} \right\rangle &= \left\langle \{n\} \left| M^0_{\mathrm{GE}} + \sum_p m_{\mathrm{GE},p} Q^{\mathrm{G}}_p + \cdots \right| \{m\} \right\rangle \\ &= M^0_{\mathrm{GE}} \boldsymbol{J}\binom{\{m\}}{\{n\}} + \sum_p m_{\mathrm{GE},p} \left\langle \{n\} | Q^{\mathrm{G}}_p | \{m\} \right\rangle + \cdots, \end{aligned} \tag{1}$$

where

$$m_{\mathrm{GE},p} = \left(\frac{\partial M_{\mathrm{GE}}}{\partial Q^{\mathrm{G}}_p} \right)_0$$

In Eq. 1, $\tilde{G}$ and $\tilde{E}$ represent the vibronic wavefunctions of the electronic ground and excited states with the respective vibrational states of $\{n\}$ and $\{m\}$. The symbols $\boldsymbol{J}\binom{\{m\}}{\{n\}}$, M^0_{GE}, $m_{\mathrm{GE},p}$, and Q^{G}_p represent the multidimensional Franck–Condon integral, the transition moment calculated at the equilibrium geometry in the electronic ground state, the linear non-Condon parameter, and the p-th normal coordinate in the ground state, respectively. The integral of the linear non-Condon term is the leading term in the weak coupling limit, which is calculated by Eq. 2,[15]

$$\begin{aligned}\left\langle \{n\} | Q^{\mathrm{G}}_p | \{m\} \right\rangle = &\left(\frac{n_p + 1}{2} \right)^{\frac{1}{2}} \boldsymbol{J}\binom{\{m\}}{\{n\} + 1_p} \\ &+ \left(\frac{n_p}{2} \right)^{\frac{1}{2}} \boldsymbol{J}\binom{\{m\}}{\{n\} - 1_p}, \end{aligned} \tag{2}$$

where n_p is the quantum number for the p-th mode. Thus, the integral is obtained by the simple Franck–Condon integrals whose vibrational quantum number of the p-th mode changes by unity.

The linear non-Condon parameter is evaluated by Eq. 3,[15]

$$m_{\mathrm{GE},p} = \sum_i \left(\frac{\partial M_{\mathrm{GE}}}{\partial \Delta X_i} \right)_0 \left(M^{-\frac{1}{2}} L_{\mathrm{G}} \right)_{ip}, \tag{3}$$

where M, L_{G}, and ΔX_i are the mass matrix, the eigenvector of the mass-weighted Cartesian force constant matrix for the ground state, and the Cartesian displacement, respectively. In the present system the mode of interest besides the totally symmetric mode (a_1) is the in-plane non-totally symmetric mode (b_2) which couples the two electronic states of $^2A_2$ and $^2B_1$ symmetries so that the Cartesian displacement is limited within the molecular plane. The gradient $(\partial M_{\mathrm{GE}}/\partial \Delta X_i)_0$ is calculated numerically by the differentiation of the transition moment as a function of the Cartesian displacement around the equilibrium geometry in the ground state. In the present calculation, the transition moment is calculated by the multi-reference single and double excitation configuration interaction (MR-SD-CI) procedure with the Huzinaga–Dunning DZV basis set: (9s5p/4s)/[3s2p/2s]. The program employed is MELDF.[18] The reference configurations are chosen by the criterion that the CI coefficients exceed 0.1, which include $[\cdots(1b_1)^2(2b_1)^2(8b_2)^2(1a_2)^2(3b_1)^1]$, $[\cdots(1b_1)^2(2b_1)^1(8b_2)^2(1a_2)^2(3b_1)^2]$, $[\cdots(1b_1)^2(2b_1)^1$

$(8b_2)^2(1a_2)^2(3b_1)^1(4b_1)^1]$, and $[\cdots(1b_1)^2(2b_1)^2(8b_2)^2(1a_2)^2(3b_1)^0(4b_1)^1]$ for the $^2B_1$ states and $[\cdots(1b_1)^2(2b_1)^2(8b_2)^2(1a_2)^1(3b_1)^2]$, $[\cdots(1b_1)^2(2b_1)^2(8b_2)^2(1a_2)^1(3b_1)^1(4b_1)^1]$, $[\cdots(1b_1)^2(2b_1)^2(8b_2)^2(1a_2)^2(3b_1)^0(2a_2)^1]$, and $[\cdots(1b_1)^2(2b_1)^1(8b_2)^2(1a_2)^2(3b_1)^1(2a_2)^1]$ for the $^2A_2$ states. The molecular orbitals $1b_1$—$5b_1$, $1a_2$—$2a_2$, and $8b_2$ correspond to the seven π and π^* and one n orbitals which are shown in Fig.2 of Ref. 1. The total number of the configurations in the CI wavefunction after the perturbation selection is about 8000. The weights of the reference configurations listed above for the converged CI states are found as follows: 0.85, 0.01, 0.02, and 0.01 for $\tilde{X}\,^2B_1$; 0.03, 0.37, 0.30, and 0.18 for $\tilde{1}\,^2A_2$; 0.64, 0.16, 0.08, and 0.06 for $\tilde{2}\,^2B_1$.

The absorption intensity is described by Eq. 4:

$$I_{0\to\{m\}} = \left(E_{GE} + \varepsilon_m^E\right)\left|M_{GE}^0 \boldsymbol{J}\binom{\{m\}}{0} + \frac{1}{\sqrt{2}}\sum_{p'} m_{GE,p'}\boldsymbol{J}\binom{\{m\}}{1_{p'}}\right|^2, \quad (4)$$

where E_{GE} and ε_m^E are the electronic and the vibrational energies, respectively. The second term in the squared factor represents the contribution from the vibronic coupling.

The Raman intensity is given by Eq. 5:[15]

$$I_{0\to 1_p} = E_L E_S^3 \sum_{E_i} |\, A + B\,|^2, \quad (5)$$

$$A = {M_{GE_i}^0}^2 \sum_{\{m\}} \frac{\boldsymbol{J}\binom{\{m\}}{0}\boldsymbol{J}\binom{\{m\}}{1_p}}{\varepsilon_m^{E_i} - \varepsilon_0^G + E_{GE_i} - E_L - i\Gamma}, \quad (6a)$$

$$B = M_{GE_i}^0 \sum_{p'} m_{GE,p'} \sum_{\{m\}} \frac{1}{\varepsilon_m^{E_i} - \varepsilon_0^G + E_{GE_i} - E_L - i\Gamma} \times \left[\boldsymbol{J}\binom{\{m\}}{0}\left\{\boldsymbol{J}\binom{\{m\}}{2_{p'}} + \frac{1}{\sqrt{2}}\boldsymbol{J}\binom{\{m\}}{0}\right\} + \boldsymbol{J}\binom{\{m\}}{1_p}\boldsymbol{J}\binom{\{m\}}{1_{p'}}\right]. \quad (6b)$$

In Eqs. 5, 6a, and 6b, E_{GE} stands for the electronic transition energy with which the pump laser is in resonance. In the case of the phenoxy radical absorbing at ca.400 nm, the two transitions $\tilde{X}\,^2B_1 \to \tilde{1}\,^2A_2$ and $\tilde{X}\,^2B_1 \to \tilde{2}\,^2B_1$ are nearly resonant transitions. E_L and E_S are the incident and scattered photon energies. Γ is the homogeneous linewidth. The contribution from the vibronic coupling is represented by the B-term.

The force constants in the present calculation are the same as those in our previous work[1] calculated by ab initio MO methods and scaled by comparing with the experimental TIP and Raman spectra. The optimized geometries obtained in the previous work are used in the present work. The multidimensional Franck–Condon integrals with the Duschinsky effect being taken into account are calculated by the recurrence formulae,[19,20] where the k-vector is modified by the "scaling of the geometry factor" of 0.8 as is described in the previous work.[1]

Results and Discussion

Linear Non-Condon Parameters. For the calculation of the linear non-Condon parameters, the differential coefficient $(\partial M_{GE}/\partial \Delta X_i)_0$ is first calculated by the MR-SD-CI procedure described above. The Cartesian displacement is chosen to be 0.05 bohr or less, thus the changes in the CI coefficients of the reference configurations remain within 5% of the CI coefficients in the equilibrium geometry. The linear non-Condon parameters are then calculated by Eq. 3.

The transition moments for the equilibrium geometry of the ground state are calculated as 0.37950 and 0.26474 a.u. for $\tilde{X}\,^2B_1 \to \tilde{1}\,^2A_2$ and $\tilde{X}\,^2B_1 \to \tilde{2}\,^2B_1$, respectively.[1] The results of the calculation of the linear non-Condon parameter for the totally symmetric modes (a_1) and the in-plane non-totally symmetric modes (b_2) are shown in Table 1. In order to adjust the theoretical absorption and Raman spectra with the experimental, we have scaled the ab initio linear non-Condon parameters by multiplying the transition moments of the ground state in the equilibrium geometry by scaling constants. The scaled parameters are shown in Table 1 along with the ab initio parameters.

It is seen that the scaled linear non-Condon parameters for $\tilde{X}\,^2B_1 \to \tilde{1}\,^2A_2$ and $\tilde{X}\,^2B_1 \to \tilde{2}\,^2B_1$, $m_{GE_1,p}$ and $m_{GE_2,p}$, are crudely related as follows:

$$m_{GE_1,p} \approx -m_{GE_2,p} \quad (7)$$

This relation is rationalized by the following argument.

For a molecule with three electronic states $\tilde{G}$, $\tilde{E}_1$, and

Table 1. Linear Non-Condon Parameter

Mode	$\tilde{X}\,^2B_1 \to \tilde{1}\,^2A_2$		$\tilde{X}\,^2B_1 \to \tilde{2}\,^2B_1$	
	Ab initio	Scaled	Ab initio	Scaled
$1a_1$	0.01891	0.01518	−0.04043	−0.02647
$2a_1$	−0.02562	−0.04554	0.03878	0.02647
$3a_1$	−0.03407	−0.04554	0.00859	0.01059
$4a_1$	−0.05463	−0.01518	−0.02913	0.01588
$5a_1$	0.07647	0.04554	−0.07006	−0.02118
$6a_1$	−0.00818	−0.00759	−0.00495	0.01588
$7a_1$	−0.01969	0.03795	−0.02150	−0.01588
$8a_1$	−0.03180	−0.03036	0.01426	0.00529
$9a_1$	0.01099	0.00759	−0.04022	−0.03706
$10a_1$	0.03891	0.03036	−0.01009	−0.01059
$11a_1$	−0.04149	−0.02277	0.02101	0.02647
$1b_2$	0.00545	0.00759	−0.00508	−0.00529
$2b_2$	−0.03654	−0.03795	0.02517	0.02118
$3b_2$	0.02387	0.05313	0.02337	−0.02647
$4b_2$	0.01969	0.05313	−0.01055	−0.02647
$5b_2$	0.05693	0.01518	−0.02041	−0.01059
$6b_2$	−0.01438	0.03795	0.02093	−0.01588
$7b_2$	0.06984	0.02277	−0.01341	−0.01059
$8b_2$	−0.07457	−0.05313	0.00988	0.04236
$9b_2$	−0.00554	−0.02277	0.00656	0.01588
$10b_2$	0.05546	0.03795	−0.01852	−0.01059

$\tilde{E}_2$, the conventional Herzberg–Teller expansion leads to Eqs. 8a and 8b:

$$\phi_G = \phi_G^0 + \sum_p \frac{\lambda_p^{GE_1} Q_p}{E_G^0 - E_{E_1}^0} \phi_{E_1}^0 + \sum_p \frac{\lambda_p^{GE_2} Q_p}{E_G^0 - E_{E_2}^0} \phi_{E_2}^0, \quad (8a)$$

$$\phi_{E_1} = \phi_{E_1}^0 + \sum_p \frac{\lambda_p^{GE_1} Q_p}{E_{E_1}^0 - E_G^0} \phi_G^0 + \sum_p \frac{\lambda_p^{E_1E_2} Q_p}{E_{E_1}^0 - E_{E_2}^0} \phi_{E_2}^0, \quad (8b)$$

where λ_p represents the vibronic coupling constant. Then, the electronic transition moment for $\tilde{X}\,^2B_1 \rightarrow \tilde{1}\,^2A_2$ is approximated by Eq. 9:

$$\begin{aligned} M_{GE_1} = M_{GE_1}^0 &+ \sum_p \frac{\lambda_p^{E_1E_2} Q_p}{E_{E_1}^0 - E_{E_2}^0} M_{GE_2}^0 \\ &+ \sum_p \frac{\lambda_p^{GE_2} Q_p}{E_G^0 - E_{E_2}^0} M_{E_2E_1}^0 + \sum_p \frac{\lambda_p^{GE_1} Q_p}{E_{E_1}^0 - E_G^0} M_{GG}^0 \\ &+ \sum_p \frac{\lambda_p^{GE_1} Q_p}{E_G^0 - E_{E_1}^0} M_{E_1E_1}^0 + \boldsymbol{O}(Q^2). \end{aligned} \quad (9)$$

In the right hand side of Eq. 9, the third, fourth, and fifth terms are much smaller than the second term because $|E_{E_1}^0 - E_{E_2}^0| \ll E_G^0 - E_{E_1}^0$ and $|E_{E_1}^0 - E_{E_2}^0| \ll E_G^0 - E_{E_2}^0$ ($|E_{E_1}^0 - E_{E_2}^0| \cong 1100$ cm^{-1}, $E_G^0 - E_{E_1}^0 \cong E_G^0 - E_{E_2}^0 \cong 25000$ cm^{-1}). Therefore, only the second term contributes significantly to the linear non-Condon term to give the linear non-Condon parameters for $\tilde{X}\,^2B_1 \rightarrow \tilde{1}\,^2A_2$ and $\tilde{X}\,^2B_1 \rightarrow \tilde{2}\,^2B_1$ by Eqs. 10a and 10b, respectively.

$$m_{GE_1} \cong \frac{\lambda_p^{E_1E_2}}{E_{E_1}^0 - E_{E_2}^0} M_{GE_2}^0, \quad (10a)$$

$$m_{GE_2} \cong \frac{\lambda_p^{E_1E_2}}{E_{E_2}^0 - E_{E_1}^0} M_{GE_1}^0. \quad (10b)$$

Since $M_{GE_1}^0$ and $M_{GE_2}^0$ are nearly equal, one obtains the relation in Eq. 7. The deviation from the exact equality in Eq. 7 is interpreted as due to the contributions from the third, fourth, and fifth terms of Eq. 9 as well as from electronic states other than the three states.

Absorption Spectrum. The absorption spectrum without considering the vibronic coupling is calculated by the first term alone in the squared factor of Eq. 4. In this case, only the fundamental, overtone, and combination bands of the totally symmetric modes of the excited states possess significant intensities. The intensities of the bands originating from the overtone and combination of the non-totally symmetric modes can be non-zero, but they are negligibly small. With the vibronic coupling effect being taken into account, the contribution from the non-Condon term to the transition moment is included, and the intensities for the bands are modified accordingly. The bands with zero intensities otherwise now gain some intensities.

The force constants for the ground state and excited states are determined by comparing with the experimental Raman and TIP spectra in our previous work.[1] Recently, Sato et al. have improved the resolution of the TIP spectrum and extended the spectral region observed, as shown in Fig. 1 (a).[12] The theoretical absorption spectrum by the simple superposition of the transitions $\tilde{X}\,^2B_1 \rightarrow \tilde{1}\,^2A_2$ and $\tilde{X}\,^2B_1 \rightarrow \tilde{2}\,^2B_1$ without taking into account of the vibronic coupling is shown in Fig. 1 (b), whereas the spectrum including the vibronic coupling effect is shown in Fig. 1 (c). The characters of the normal modes $1a_1$ through $11a_1$ are given in Table 4 and Fig.3 in our previous work.[1] The stick spectra for Fig. 1 (b) and (c) and the assignment of the spectrum in Fig. 1 (a) are shown in Table 2. In Fig. 1 (b) and (c) each peak is broadened rather arbitrarily with a Lorentzian linewidth of 20 cm^{-1}. In Fig. 1 (b) the ratio of the 0–0 bands of the two transitions are taken to be 100 : 80 to be consistent with Fig. 1 (a).

In Fig. 1 (a), peaks 2 and 3 are regarded as due to the intermolecular vibration of the parent complex $[C_6H_5OH\text{–}N(CH_3)_3]^+$.[12] Peak 10 may be a superposition of the intermolecular vibration and a fundamental vibronic band of the phenoxy radical (see Table 2).[12] In the present calculation dealing with the free phenoxy radical, the bands originating from the intermolecular vibration observed in the TIP spectrum are neglected. Due to the presence of the background absorption in Fig. 1 (a), the comparison between the experimental and calculated absorption intensities is not straightforward. However, it is notable that the intensities for peaks 10, 12—14, and 16—20 are improved by going from Fig. 1 (b) to Fig. 1 (c) as compared with Fig. 1 (a), even if the improvement is rather modest. It should be noted that the improvement cannot be drastic, because the present treatment is based upon the weak coupling limit.

As for the bands whose intensities are zero in the absence of the vibronic coupling, the intensities after the inclusion of the effect of the vibronic coupling still remain small, because the second term in the squared factor of Eq. 4 is smaller by one order of magnitude than the first and so the intensities due to the second term become smaller than that for the totally-symmetric modes by two orders of magnitude.

The contribution from various normal modes to the vibronic coupling effect is shown in Table 3. The non-Condon terms of only the totally symmetric modes, $4a_1$ through $11a_1$, are counted because the remaining $1a_1$ through $3a_1$ are for C–H stretching (see Table 5 of Ref. 1) and their contribution is negligible. It is seen that only one or two particular modes contribute dominantly: e.g., mode $10a_1$ to band $10a_1$, modes $7a_1$ and $8a_1$ to band $7a_1$, mode $5a_1$ to band $6a_1$, and modes $5a_1$ and $7a_1$ to band $4a_1$ for $\tilde{X}\,^2B_1 \rightarrow \tilde{1}\,^2A_2$. Similarly, mode $11a_1$ to band $11a_1$, mode $9a_1$ to band $10a_1$, mode $9a_1$ to band $9a_1$, mode $7a_1$ to band $7a_1$ for $\tilde{X}\,^2B_1 \rightarrow \tilde{2}\,^2B_1$.

Raman Spectrum. The intensity of the Raman spectrum is obtained as the sum of the contributions from the two transitions. In the treatment without the vibronic coupling, the Raman intensities are obtained by the *A*-term only, so that the intensities of only the totally symmetric modes are non-zero, whereas in the

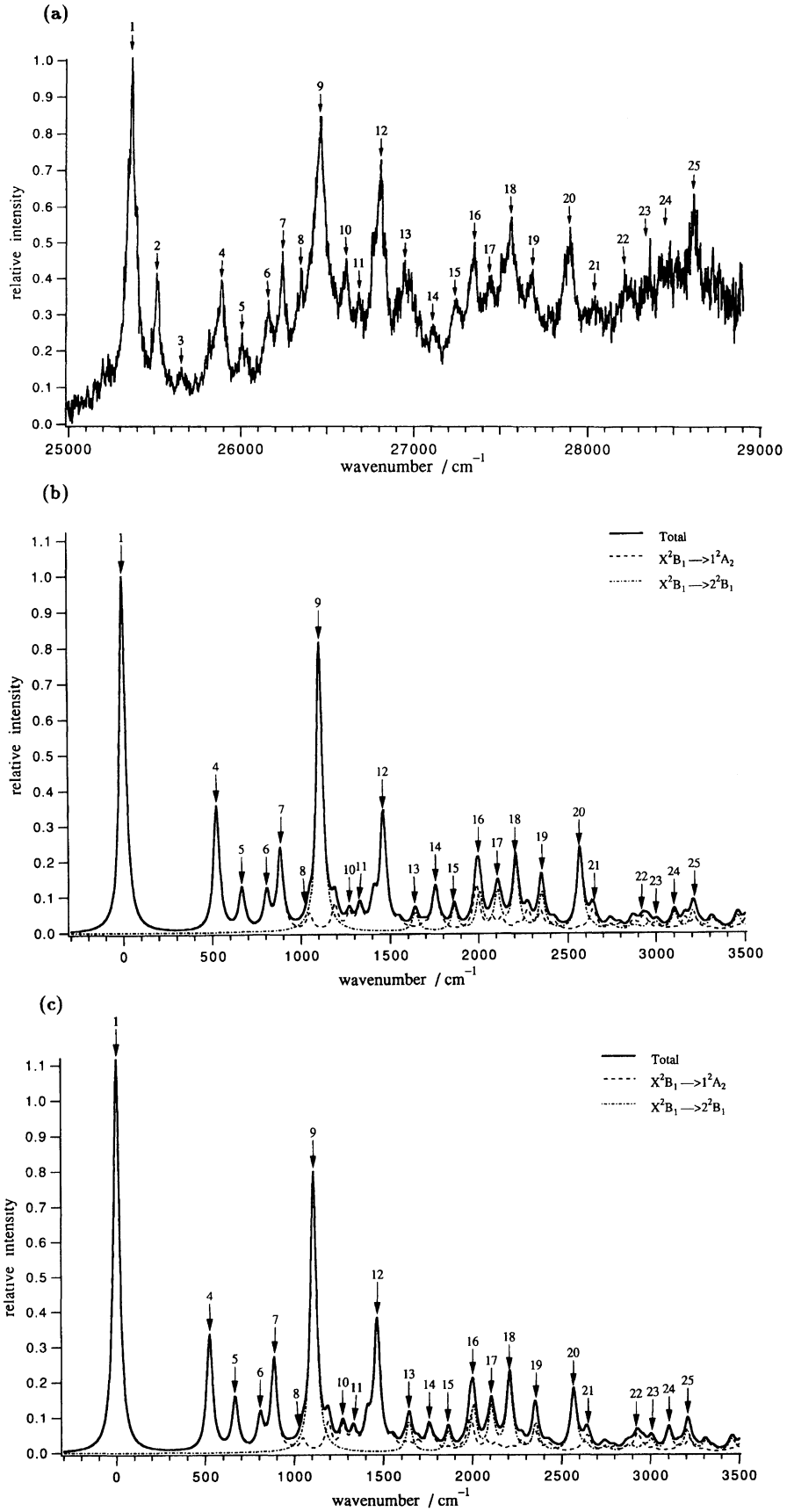

Fig. 1. The absorption spectrum. (a) TIP spectrum of $[C_6H_5OH\text{–}N(CH_3)_3]^+$ reproduced from Ref. 12. (b) The theoretical absorption spectrum constructed without taking into account the vibronic coupling. (c) The theoretical absorption spectrum with the vibronic coupling.

Table 2. Vibronic Absorption Spectrum

Peak no. in Fig.1(a)	Expl. wavenumber cm^{-1}	Assignment	Calcd wavenumber cm^{-1}	Relative intensity[a)]	Relative intensity[b)]
1	0	$\tilde{1}^2A_2$ 0–0 band	0	1.000	1.115
2	150	$\tilde{1}^2A_2$ 0–0 band + σ_ν[c)]	—	—	—
3	295	$\tilde{1}^2A_2$ 0–0 band + $\sigma_\nu \times 2$	—	—	—
4	531	$\tilde{1}^2A_2$ 11 a_1	525	0.352	0.330
5	647	$\tilde{1}^2A_2$ 10 a_1	667	0.115	0.148
6	799	$\tilde{1}^2A_2$ 9 a_1	807	0.102	0.095
7	881	$\tilde{1}^2A_2$ 8 a_1	885	0.223	0.256
8	994	$\tilde{1}^2A_2$ 7 a_1	979	0.001	0.005
9	1101	$\tilde{1}^2A_2$ 11 $a_1 \times 2$	1050	0.045	0.033
9	1101	$\tilde{2}^2B_1$ 0–0 band	1110 (0)	0.800	0.786
9	1101	$\tilde{1}^2A_2$ 10 a_1+11 a_1	1192	0.071	0.079
10	1253	$\tilde{2}^2B_1$ 0–0 band + σ_ν	—	—	—
10	1253	$\tilde{1}^2A_2$ 6 a_1	1272	0.043	0.068
11	1325	$\tilde{1}^2A_2$ 9 a_1 + 11 a_1	1332	0.060	0.050
12	1446	$\tilde{1}^2A_2$ 8 a_1 + 11 a_1	1410	0.082	0.080
12	1446	$\tilde{1}^2A_2$ 5 a_1	1463	0.304	0.341
12	1446	$\tilde{1}^2A_2$ 9 a_1 + 10 a_1	1474	0.030	0.033
13	1630 (529)	$\tilde{2}^2B_1$ 11 a_1	1642 (532)	0.052	0.085
14	1749	$\tilde{1}^2A_2$ 4 a_1	1754	0.108	0.064
15	1884 (783)	$\tilde{2}^2B_1$ 10 a_1	1863 (753)	0.067	0.055
16	1991	$\tilde{1}^2A_2$ 5 a_1 + 11 a_1	1987	0.110	0.103
16	1991 (890)	$\tilde{2}^2B_1$ 9 a_1	2006 (896)	0.107	0.128
17	2082 (981)	$\tilde{2}^2B_1$ 8 a_1	2108 (998)	0.105	0.123
18	2201 (1100)	$\tilde{2}^2B_1$ 7 a_1	2209 (1099)	0.189	0.205
19	2327	$\tilde{1}^2A_2$ 5 a_1 + 8 a_1	2347	0.055	0.055
19	2327 (1226)	$\tilde{2}^2B_1$ 6 a_1	2354 (1244)	0.103	0.077
20	2540 (1439)	$\tilde{2}^2B_1$ 5 a_1	2568 (1458)	0.220	0.169
21	~2650	$\tilde{1}^2A_2$ 4 a_1 + 8 a_1	2639	0.043	0.031
22	~2900	$\tilde{1}^2A_2$ 5 $a_1 \times 2$	2924	0.043	0.048
23	~3000 (~1900)	$\tilde{2}^2B_1$ 4 a_1	3011 (1901)	0.001	0.008
24	~3100 (~2000)	$\tilde{2}^2B_1$ 7 a_1 + 9 a_1	3105 (1995)	0.030	0.035
25	~3250 (~2150)	$\tilde{2}^2B_1$ 7 a_1 + 8 a_1	3207 (2097)	0.050	0.058
25	~3250	$\tilde{1}^2A_2$ 4 a_1 + 5 a_1	3216	0.030	0.031

a) The relative intensity without the vibronic coupling in Fig. 1 (b). b) The relative intensity with the vibronic coupling in Fig. 1 (c). c) The intermolecular stretching of $[Phenol\text{–}N(CH_3)_3]^+$.

The numbers in parentheses are the wavenumbers which are measured from the 0–0 band of the $\tilde{2}\,^2B_1$ state. The assignments in the third column for the same peak number are intended to imply that the peak comprises several superposing vibronic bands.

treatment including the vibronic coupling, the intensities of the non-totally modes are also non-zero.

The experimental Raman spectrum of the phenoxy radical excited at 399 nm obtained by Tripathi and Schuler is shown in Fig. 2 (a).[9,10] The theoretical Raman spectrum is calculated by using the same set of the force constants as the absorption spectrum. The results without and with the vibronic coupling are shown in Fig. 2 (b) and (c), respectively. The stick spectra for the figures are shown in Table 4. The values of E_{GE} for $\tilde{X}\,^2B_1 \rightarrow \tilde{1}\,^2A_2$ and $\tilde{X}\,^2B_1 \rightarrow \tilde{2}\,^2B_1$, are taken to be 26400 cm^{-1} and 27510 cm^{-1}, respectively, and the values of E_L and Γ to be 25000 cm^{-1} and 70 cm^{-1}. The ratio of M^0_{XA} and M^0_{XB} is set as $M^0_{XA} : M^0_{XB} = 10 : 9$ to be consistent with the ratio of the oscillator strengths of the theoretical absorption spectrum in Fig. 1 (b). It is noted that the above ratio of M^0_{XA} and M^0_{XB} is fairly close to the ratio of the calculated transition moment of $0.3795 : 0.2647 \approx 10 : 7$. The values of m_{GE} are normalized to be consistent with the ratio of M^0_{XA} and M^0_{XB}. As the virtual states, all the fundamental, overtone, and combination states of the totally and non-totally symmetric modes are included. In Fig. 2 (b) and (c) each peak is broadened with a Lorentzian linewidth of 15 cm^{-1}.

The theoretical spectra exhibit more peaks than the experimental, which may be attributable to the obliteration of the weak peaks in the experimental spectrum due to the presence of emission. We also have to admit that the use of a common value of the Lorentzian linewidth of 15 cm^{-1} may not be appropriate. Despite these deficiencies, it is seen that Fig. 2 (c) reproduces the experimental spectrum better than Fig. 2 (b) in several points; the bands assigned as $8a_1$ (995 cm^{-1}),

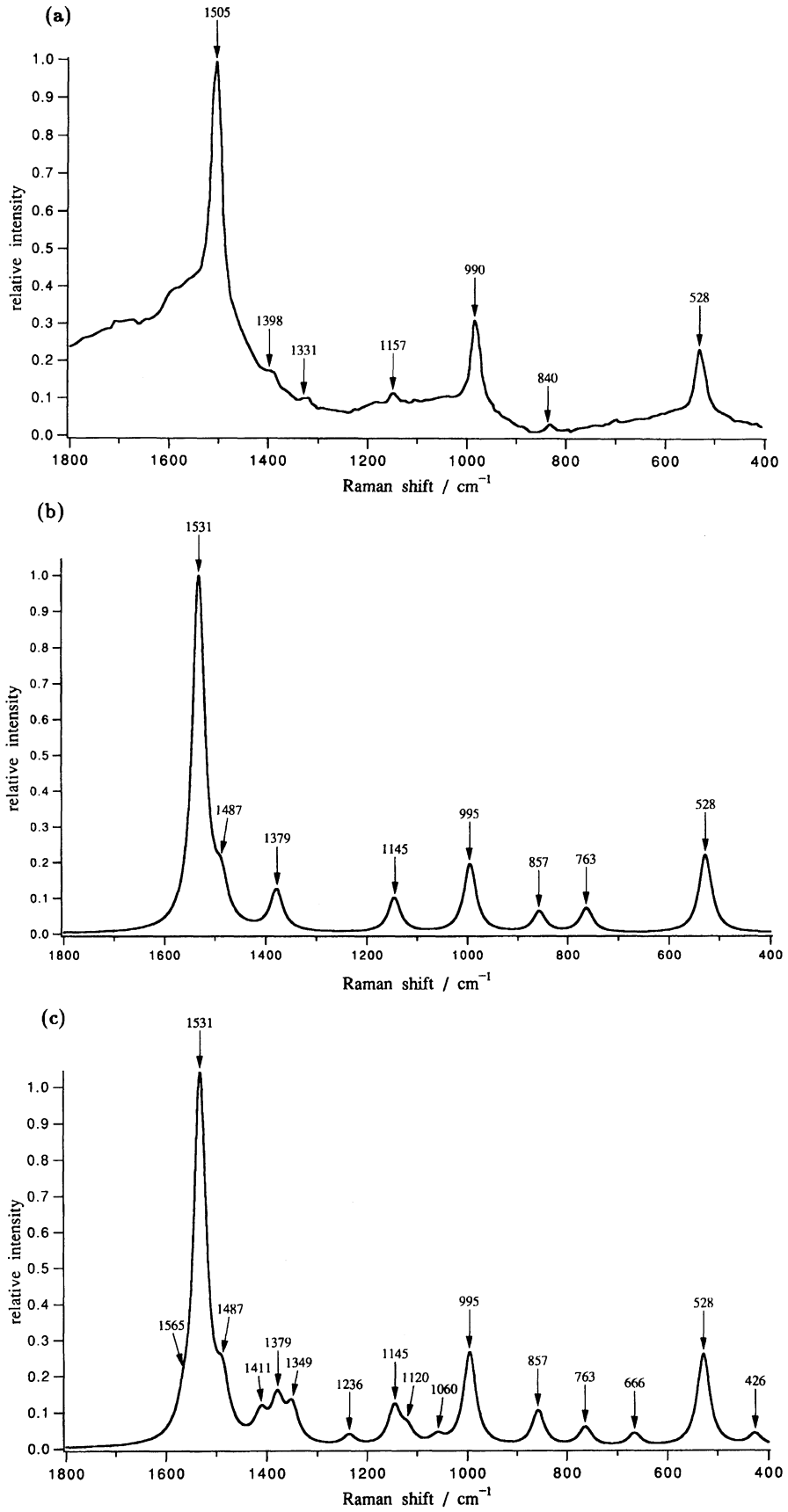

Fig. 2. The Raman spectrum. (a) Transient Raman spectrum of the phenoxy-h_5 radical resonanced at 399 nm reproduced from Ref. 9. (b) The theoretical Raman spectrum constructed without taking into account the vibronic coupling. (c) The theoretical Raman spectrum with the vibronic coupling.

Table 3. Non-Condon Terms in the Absorption Intensity

Excitation	Frequency	Zeroth-order	Non-Condon	Division of non-Condon term							
	cm^{-1}	term	term	$4a_1$	$5a_1$	$6a_1$	$7a_1$	$8a_1$	$9a_1$	$10a_1$	$11a_1$
$\tilde{1}^2A_2$ 0–0	0	1.0000	0.0562	0.0079	0.0106	0.0049	−0.0145	0.0037	0.0064	0.0072	0.0300
$\tilde{1}^2A_2$ $11a_1$	525	−0.5866	0.0184	−0.0037	−0.0147	−0.0029	0.0117	−0.0012	−0.0070	0.0162	0.0200
$\tilde{1}^2A_2$ $10a_1$	667	0.3347	0.0452	0.0018	0.0154	0.0025	−0.0148	0.0074	−0.0044	0.0444	−0.0070
$\tilde{1}^2A_2$ $9a_1$	807	−0.3152	0.0122	−0.0033	0.0423	−0.0018	−0.0367	0.0274	−0.0014	−0.0126	−0.0017
$\tilde{1}^2A_2$ $8a_1$	884	−0.4640	−0.0331	−0.0035	−0.0231	−0.0021	−0.0176	−0.0047	0.0080	0.0235	−0.0138
$\tilde{1}^2A_2$ $7a_1$	979	−0.0083	0.0780	0.0031	−0.0034	−0.0048	0.0361	0.0404	0.0026	0.0072	−0.0032
$\tilde{1}^2A_2$ $6a_1$	1273	−0.2020	−0.0517	0.0002	−0.0506	0.0078	−0.0108	0.0230	−0.0033	−0.0096	−0.0084
$\tilde{1}^2A_2$ $5a_1$	1462	−0.5350	−0.0317	0.0093	0.0051	−0.0029	−0.0032	−0.0127	−0.0042	−0.0046	−0.0185
$\tilde{1}^2A_2$ $4a_1$	1754	0.3182	−0.0738	0.0021	−0.0390	−0.0082	−0.0341	0.0030	−0.0013	−0.0038	0.0075
$\tilde{2}^2B_1$ 0–0	0	1.0000	−0.0086	0.0253	0.0098	0.0158	−0.0029	−0.0054	−0.0347	−0.0088	−0.0077
$\tilde{2}^2B_1$ $11a_1$	532	−0.2541	−0.0676	−0.0051	−0.0011	−0.0001	0.0015	0.0019	0.0050	−0.0026	−0.0671
$\tilde{2}^2B_1$ $10a_1$	753	0.2855	−0.0275	0.0035	0.0021	−0.0005	−0.0043	−0.0024	−0.0353	0.0239	−0.0144
$\tilde{2}^2B_1$ $9a_1$	896	0.3590	0.0346	0.0040	−0.0034	−0.0045	−0.0122	−0.0074	0.0683	−0.0001	−0.0101
$\tilde{2}^2B_1$ $8a_1$	998	0.3551	0.0300	0.0112	0.0117	0.0043	−0.0187	0.0100	0.0146	−0.0004	−0.0026
$\tilde{2}^2B_1$ $7a_1$	1099	−0.4756	−0.0199	−0.0129	0.0074	0.0127	−0.0307	−0.0019	−0.0037	0.0022	0.0070
$\tilde{2}^2B_1$ $6a_1$	1244	−0.3505	0.0469	0.0140	−0.0353	0.0179	0.0047	0.0025	0.0306	0.0083	0.0043
$\tilde{2}^2B_1$ $5a_1$	1458	0.5106	−0.0633	−0.0203	−0.0256	0.0184	−0.0026	−0.0005	−0.0227	−0.0061	−0.0038
$\tilde{2}^2B_1$ $4a_1$	1901	0.0029	0.0979	−0.0106	0.0309	0.0237	0.0168	0.0002	0.0305	0.0048	0.0016

The relative values for the zeroth-order and non-Condon terms in the absorption intensity (the first and the second terms in the squared factor in Eq. 4) are shown, where the values of the zeroth-order term for the respective 0–0 bands of the excitations are set as 1.0.

Table 4. Raman Spectrum

	Raman frequency/cm^{-1}		Relative intensity without the vibronic coupling in Fig. 2 (b)			Relative intensity with the vibronic coupling in Fig. 2 (c)		
Mode	Exptl	Calcd	Total	$\tilde{X}\,^2B_1 \rightarrow \tilde{1}\,^2A_2$	$\tilde{X}\,^2B_1 \rightarrow \tilde{2}\,^2B_1$	Total	$\tilde{X}\,^2B_1 \rightarrow \tilde{1}\,^2A_2$	$\tilde{X}\,^2B_1 \rightarrow \tilde{2}\,^2B_1$
$3b_2$	—	1565	0	0	0	0.05251	0.05158	0.00093
$4a_1$	1505	1531	1.00000	0.92072	0.07928	1.02847	0.94729	0.08118
$5a_1$	—	1487	0.10816	0.10168	0.00648	0.14073	0.13794	0.00279
$4b_2$	—	1411	0	0	0	0.07200	0.07101	0.00099
$6a_1$	1398	1379	0.11537	0.06622	0.04915	0.11716	0.06264	0.05452
$5b_2$	1331	1349	0	0	0	0.09675	0.09520	0.00155
$6b_2$	—	1236	0	0	0	0.02905	0.02763	0.00142
$7a_1$	1157	1145	0.09776	0.09741	0.00035	0.10788	0.10610	0.00178
$7b_2$	—	1120	0	0	0	0.04145	0.03992	0.00153
$8b_2$	—	1060	0	0	0	0.02423	0.02051	0.00372
$8a_1$	990	995	0.19431	0.16090	0.03341	0.26341	0.23751	0.02590
$9a_1$	840	857	0.05940	0.01999	0.03941	0.09972	0.04230	0.05742
$10a_1$	—	763	0.06853	0.01696	0.05157	0.05339	0.01212	0.04127
$9b_2$	—	666	0	0	0	0.03615	0.03285	0.00330
$11a_1$	528	528	0.22092	0.19622	0.02470	0.25912	0.22325	0.03587
$10b_2$	—	426	0	0	0	0.03468	0.03275	0.00193

$9a_1$ (857 cm^{-1}), and $11a_1$ (528 cm^{-1}) are intensified, whereas the $10a_1$ (763 cm^{-1}) band is suppressed. It is also found that the non-totally symmetric modes gain unignorable Raman intensities. In particular, the intensities of the $4b_2$ (1411 cm^{-1}) and $5b_2$ (1349 cm^{-1}) bands are similar to that of the $6a_1$ (1379 cm^{-1}) band appearing in between them. The $5b_2$ (1349 cm^{-1}) band is considered to correspond to the peak observed at 1331 cm^{-1}. The apparent absence of the peak corresponding to the theoretical $4b_2$ (1411 cm^{-1}) band in the observed spectrum may be considered to indicate that the peak has been burried the strong peak at 1505 cm^{-1} and the background emission. The same may be said about the $5a_1$ (1487 cm^{-1}) and $3b_2$ (1565 cm^{-1}) peaks.

The Raman intensity can be decomposed into several components, as shows in Table 5. The *B*-term originating from the non-totally symmetric modes becomes a constant for the totally symmetric modes, and vice versa. It is seen that the non-totally symmetric modes contribute significantly in the *B*-term of the totally

Table 5. Components of the Raman Intensity

Mode	Raman frequency / cm^{-1}		$\tilde{X}\,^2B_1 \rightarrow \tilde{1}\,^2A_2$					$\tilde{X}\,^2B_1 \rightarrow \tilde{2}\,^2B_1$				
			Real part			Imaginary part		Real part			Imaginary part	
	Exptl	Calcd	*A*-term	*B*-term (sym)	*B*-term (asym)	*A*-term	*B*-term (sym)	*B*-term (asym)	*A*-term	*B*-term (sym)	*B*-term (asym)	*A*-term	*B*-term (sym)	*B*-term (asym)
$4a_1$	1505	1531	0.3903	0.0136	−0.0131	0.1829	0.0018	0.0113	−0.1220	0.0086	−0.0088	0.0332	−0.0004	0.0050
$5a_1$	—	1487	−0.1343	−0.0063	−0.0131	0.0486	0.0038	0.0113	0.0348	−0.0030	−0.0088	−0.0095	−0.0011	0.0050
$6a_1$	1398	1379	0.0110	−0.0310	−0.0131	0.1139	−0.0036	0.0113	−0.0971	0.0042	−0.0088	0.0171	−0.0011	0.0050
$7a_1$	1157	1145	−0.0260	0.0247	−0.0131	0.1343	−0.0035	0.0113	−0.0062	−0.0008	−0.0088	0.0053	−0.0010	0.0050
$8a_1$	990	995	−0.1720	−0.0216	−0.0131	−0.0275	−0.0290	0.0113	0.0761	0.0000	−0.0088	−0.0225	−0.0014	0.0050
$9a_1$	840	857	−0.0416	−0.0090	−0.0131	0.0444	0.0057	0.0113	−0.0836	−0.0086	−0.0088	0.0176	−0.0018	0.0050
$10a_1$	—	763	−0.0112	−0.0033	−0.0131	−0.0546	0.0051	0.0113	−0.0967	0.0161	−0.0088	0.0097	−0.0023	0.0050
$11a_1$	528	528	−0.1818	0.0052	−0.0131	−0.0432	−0.0292	0.0113	0.0065	0.0210	−0.0088	0.0094	0.0038	0.0050
$3b_2$	—	1565	0	−0.0023	0.0059	0	−0.0043	0.1085	0	0.0009	0.0087	0	−0.0010	−0.0067
$4b_2$	—	1411	0	−0.0023	−0.0570	0	−0.0043	0.1092	0	0.0009	0.0090	0	−0.0010	−0.0068
$5b_2$	1331	1349	0	−0.0023	−0.1183	0	−0.0043	0.0713	0	0.0009	0.0134	0	−0.0010	−0.0063
$6b_2$	—	1236	0	−0.0023	−0.0458	0	−0.0043	0.0615	0	0.0009	0.0125	0	−0.0010	−0.0062
$7b_2$	—	1120	0	−0.0023	−0.0465	0	−0.0043	0.0788	0	0.0009	0.0130	0	−0.0010	−0.0063
$8b_2$	—	1060	0	−0.0023	−0.0197	0	−0.0043	0.0647	0	0.0009	0.0235	0	−0.0010	−0.0058
$9b_2$	—	666	0	−0.0023	−0.0388	0	−0.0043	0.0715	0	0.0009	0.0216	0	−0.0010	−0.0046
$10b_2$	—	426	0	−0.0023	−0.0433	0	−0.0043	0.0670	0	0.0009	0.0030	0	−0.0010	−0.0157

The relative values for the *A*-term and *B*-term in Eqs. 6a and 6b, respectively, are shown. The *B*-term is divided to the two parts according to the contribution from the totally symmetric modes (sym) or the non-totally symmetric modes (asym).

symmetric modes, while the totally symmetric modes contribute only slightly to the non-totally symmetric modes.

Conclusion

The vibronic coupling effect in the absorption and Raman spectra for the ca.400 nm band of the phenoxy radical was studied by ab initio MO calculations. The effect is treated in the weak coupling limit. The absorption and Raman spectra for the ca.400 nm band is approximated by the simple sum of the two transitions $\tilde{X}\,^2B_1 \rightarrow \tilde{1}\,^2A_2$ and $\tilde{X}\,^2B_1 \rightarrow \tilde{2}\,^2B_1$ and the effect is represented as the additional intensities originating from the linear non-Condon term in the absorption spectrum and from the *B*-term in the Raman spectrum. The non-Condon parameters are calculated by an MR-SD-CI procedure and scaled in reference to the experimental spectra. The ab initio force constants which are scaled by referring to the experimental resonance Raman and Trapped Ion Photodissociation (TIP) spectra in the previous work are used in the present work. The result are summarized below.

(1) The scaled linear non-Condon parameters for $\tilde{X}\,^2B_1 \rightarrow \tilde{1}\,^2A_2$ and $\tilde{X}\,^2B_1 \rightarrow \tilde{2}\,^2B_1$ are related as $m_{GE_{1,p}} \approx -m_{GE_{2,p}}$ which is reasonable.

(2) The result of the calculation shows that the spectra which take into account the vibronic coupling effect are closer to the experimental spectra than the spectra which ignore the effect.

(3) The in-plane non-totally symmetric modes are found not to be negligible in the Raman spectrum.

The authors are grateful to Dr.Takamasa Momose for his valuable discussions. Mr. Shin Sato, Professors Takayuki Ebata and Naohiko Mikami kindly provided us pertinent experimental data of the TIP spectrum of Fig. 1 (a). Numerical calculations were performed at the Computer Center of the Kyoto University and at the IMS Computer Center. The present study was partially supported by Grants-in-Aid for Scientific Research on Priority Areas Nos. 05233108, 05237106, and 05237105 from the Ministry of Education, Science and Culture.

References

1) J. Takahashi, T. Momose, and T. Shida, *Bull. Chem. Soc. Jpn.*, **67**, 964 (1994).

2) G. Porter and E. Strachan, *Trans. Faraday Soc.*, **54**, 1595 (1958).

3) E. J. Land, G. Porter, and E. Strachan, *Trans. Faraday Soc.*, **56**, 1885 (1960).

4) J. L. Roebber, *J. Chem. Phys.*, **37**, 1974 (1962).

5) B. Ward, *Spectrochim. Acta, Part A*, **24A**, 813 (1967).

6) D. Pullin and L. Andrews, *J. Mol. Struct.*, **95**, 181 (1982).

7) S. M. Beck and L. E. Brus, *J. Chem. Phys.*, **76**, 4700 (1982).

8) C. R. Johnson, M. Ludwig, and S. A. Asher, *J. Am. Chem. Soc.*, **108**, 905 (1986).
9) G. N. R. Tripathi and R. H. Schuler, *J. Chem. Phys.*, **81**, 113 (1984).
10) G. N. R. Tripathi and R. H. Schuler, *J. Phys. Chem.*, **92**, 5129 (1988).
11) N. Mikami, T. Sasaki, and S. Sato, *Chem. Phys. Lett.*, **180**, 431 (1991).
12) S. Sato, T. Ebata, and N. Mikami, *Spectrochim. Acta, Part A*, **50A**, 1413 (1994).
13) V. B. Luzhkov and A. S. Zyubin, *J. Mol. Struct.*, **170**, 33 (1988)
14) R. Disselkamp and E. R. Bernstein, *J. Chem. Phys.*, **98**, 4339 (1993).
15) A. Warshel and P. Dauber, *J. Chem. Phys.*, **66**, 5477 (1977).
16) H. M. Lu and J. P. Page, *Chem. Phys. Lett.*, **131**, 87 (1986).
17) F. Zerbetto and M. Z. Zgierski, *Chem. Phys.*, **127**, 17 (1988).
18) E. R. Davidson et al., "Quantum Chemistry Group," Indiana University (1988), QCPE 580.
19) T. Momose and T. Shida, to be published.
20) M. Yamaguchi, T. Momose, and T. Shida, *J. Chem. Phys.*, **93**, 4223 (1990).